

This is the accepted manuscript made available via CHORUS. The article has been published as:

# Intrinsic ultralow lattice thermal conductivity of the unfilled skutterudite $\text{FeSb}_3$

Yuhao Fu, David J. Singh, Wu Li, and Lijun Zhang

Phys. Rev. B **94**, 075122 — Published 11 August 2016

DOI: [10.1103/PhysRevB.94.075122](https://doi.org/10.1103/PhysRevB.94.075122)

# Intrinsic ultralow lattice thermal conductivity of the unfilled skutterudite FeSb<sub>3</sub>

Yuhao Fu,<sup>1</sup> David J. Singh,<sup>3</sup> Wu Li,<sup>2,\*</sup> and Lijun Zhang<sup>1,†</sup>

<sup>1</sup>*College of Materials Science and Engineering and Key Laboratory of Automobile Materials of MOE, Jilin University, Changchun 130012, China*

<sup>2</sup>*Institute for Advanced Study, Shenzhen University, 3688 Nanhai Avenue, Shenzhen 518060, China*

<sup>3</sup>*Department of Physics and Astronomy, University of Missouri, Columbia, MO 65211-7010 USA*

(Dated: July 18, 2016)

It is generally accepted that unfilled skutterudites process high lattice thermal conductivity ( $\kappa_l$ ) that can be efficiently reduced upon filling. Here by using first principles Boltzmann-Peierls transport calculations, we find pure skutterudite of FeSb<sub>3</sub> with no filler in fact has an intrinsic ultralow  $\kappa_l$  smaller than that of CoSb<sub>3</sub> by one order of magnitude. The value is even smaller than those of most of the fully filled skutterudites. This finding means that with FeSb<sub>3</sub> as a reference, filling does not necessarily lower  $\kappa_l$ . The ultralow  $\kappa_l$  of FeSb<sub>3</sub> is a consequence of lowering in frequency of optical phonon branches associated with the weakly bonded Sb<sub>4</sub> rings. They overlap more with heat-carrying acoustic phonons and significantly increase the phase space for three-phonon anharmonic scattering processes. This provides an alternative non-filling related mechanism for lowering the  $\kappa_l$  of skutterudites.

PACS numbers: 72.15.Jf, 66.70.Df, 71.20.Lp, 84.60.Rb

## I. INTRODUCTION

Skutterudites are an important class of high performance thermoelectrics<sup>1–20</sup> as the embodiment of the Slack’s “electron-crystal phonon-glass” idea<sup>21</sup>. The existence of two isosahedral voids in their crystal structures allows for filling in a variety of cations (*e.g.*, rare earth, alkali earth or alkali metals). This offers dual advantages for good thermoelectrics: first, according to the Zintl concept the additional electrons transferred from the electropositive fillers to the CoSb<sub>3</sub> framework make possible flexible control of *n*-type doping<sup>4,7,8,10,11,15–17,22,23</sup>, and provides compensating change to the *p*-type doping with Co replaced by electron deficient Fe<sup>1,2,5,8,14,24</sup>. Second, and more importantly, filling strongly lowers lattice thermal conductivity ( $\kappa_l$ )<sup>1–4,7,8,10,11,15,17–19,22</sup> and optimizing the filling to lower  $\kappa_l$  both in terms of filling fraction and by using suitable mixtures of filled cations plays a central role in the optimization of high performance skutterudite thermoelectrics<sup>4</sup>.

The physical mechanism responsible for the reduction of  $\kappa_l$  in filled skutterudites remains elusive after two decades of intensive research. There are several debated aspects about the nature and role of the vibrations associated with the filled “rattling” atoms: (i) whether the motion of the rattling atoms is incoherent and non-correlated<sup>21,25–27</sup> or coherently couples with the host framework<sup>28,29</sup>; (ii) whether there exists anharmonic interaction between the localized rattling modes and the propagating phonons of the host framework<sup>30–34</sup>; (iii) whether the reduction of  $\kappa_l$  originates from the energy dissipation caused by the resonant scattering of the rattling atoms<sup>2,21,25,35</sup> or the enhanced conventional anharmonic (Umklapp) scattering processes<sup>29,33,34,36</sup>.

Despite controversy over the mechanism, there is consensus that the filling should reduce the  $\kappa_l$  of skutterudites. In this Article we report the finding via first prin-

ciples transport calculations that the recently reported skutterudite FeSb<sub>3</sub><sup>37–42</sup> often presumed to be closely related to CoSb<sub>3</sub> in fact has an very low  $\kappa_l$  without filling, even lower than those of most of the fully filled skutterudites (*e.g.*, with Ba, La and Ce). This unexpected finding indicates that filling does not necessarily lower  $\kappa_l$  of skutterudites. The ultralow  $\kappa_l$  in the unfilled FeSb<sub>3</sub> skutterudite is a consequence of lowering in frequency of optical phonon branches that take the role of the rattling modes in the filled skutterudites. The resultant optical-acoustic phonons overlapping increases three-phonon anharmonic scattering channels, thus significantly reducing phonon lifetimes and  $\kappa_l$ . Our result provides an alternative non-filling related routine to realize low  $\kappa_l$  in skutterudites.

## II. METHOD

We perform first principles calculations of  $\kappa_l$  for FeSb<sub>3</sub> and fully filled skutterudites of La/CeFe<sub>4</sub>Sb<sub>12</sub> by iteratively solving the linearized Boltzmann-Peierls transport equation of phonons with the SHENGBTE package<sup>43</sup>. The equilibrium crystal structures and interatomic force constants (IFCs) are obtained from DFT calculations with the plane-wave projector-augmented-wave method<sup>44</sup>, as implemented in the VASP code<sup>45</sup>. We employ the local density approximation (LDA) as exchange-correlation functional. A ferromagnetic configuration for FeSb<sub>3</sub> is used, which is the lowest-energy magnetic configuration at the LDA level. We did calculations with both LDA and generalized gradient approximation (GGA) functionals, and find in both cases that ferromagnetic ordering is preferred over near neighbor antiferromagnetic order. As noted in prior work by Rassander and co-workers<sup>41</sup> magnetism is important for the stability of this compound. Structural optimization is done with the kinetic energy cutoffs of 350 eV or more and the 8×8×8

$k$ -point mesh, which ensures the residual forces smaller than  $1 \times 10^{-4}$  eV/Å. The resulted equilibrium lattice constants are slightly smaller than the experimental data (by 2.03%, 1.78%, and 2.00% for FeSb<sub>3</sub>, LaFe<sub>4</sub>Sb<sub>12</sub> and CeFe<sub>4</sub>Sb<sub>12</sub>, respectively) as summarized in Table I. The agreements are reasonably good by consideration of the usual underestimation of lattice constants in the DFT-LDA calculations. The harmonic and third-order anharmonic IFCs are calculated by using the real-space supercell approach<sup>43,46</sup>, in a  $3 \times 3 \times 3$  supercell with a  $2 \times 2 \times 2$   $k$ -point mesh and a  $2 \times 2 \times 2$  supercell with a  $3 \times 3 \times 3$   $k$ -point mesh, respectively. The phonon momenta  $q$ -mesh of  $15 \times 15 \times 15$  is used in solving the transport equation to ensure  $\kappa_l$  converged at the  $1 \times 10^{-6}$  W/mK level.

TABLE I. Optimized structure parameters by total energy minimization for FeSb<sub>3</sub>, CoSb<sub>3</sub>, LaFe<sub>4</sub>Sb<sub>12</sub> and CeFe<sub>4</sub>Sb<sub>12</sub>, compared with available experimental data<sup>12,24,37</sup>.

		Lattice parameter Fractional coordinates		
		a	x	y
<b>FeSb<sub>3</sub></b>	Theory	8.968	0.329	0.161
	Exp <sup>9</sup>	9.154	0.334	0.158
<b>CoSb<sub>3</sub></b>	Theory	8.918	0.332	0.160
	Exp <sup>10</sup>	9.0345		
<b>LaFe<sub>4</sub>Sb<sub>12</sub></b>	Theory	8.985	0.335	0.164
	Exp <sup>11</sup>	9.148		
<b>CeFe<sub>4</sub>Sb<sub>12</sub></b>	Theory	8.957	0.333	0.164
	Exp <sup>11</sup>	9.140		

By solving the linearized Boltzmann-Peierls transport equation of phonons, all the contributions from two-phonon and three-phonon scattering processes responsible for intrinsic  $\kappa_l$  of crystalline materials are included. Briefly the isotopic  $\kappa_l$  of cubic skutterudites at temperature  $T$  can be represented as the sum of contributions over each phonon mode  $\lambda$  (with branch  $p$  and wave vector  $\mathbf{q}$ ):

$$\kappa_l \equiv \kappa_l^{\alpha\alpha} = \frac{1}{NV} \sum_{\lambda} C_{\lambda} v_{\lambda}^{\alpha} v_{\lambda}^{\alpha} \tau_{\lambda}, \quad (1)$$

and

$$C_{\lambda} = \frac{\partial f_{\lambda}(\omega_{\lambda}, T)}{\partial T}, \quad (2)$$

where  $N$  is the number of  $\mathbf{q}$  points uniformly sampled in the phonon Brillouin zone,  $V$  is the unit cell volume,  $C_{\lambda}$  is the phonon mode heat capacity,  $f_{\lambda}(\omega_{\lambda}, T)$  is the Bose-Einstein distribution form that is the function of the phonon frequency  $\omega_{\lambda}$  and  $T$ ,  $v_{\lambda}^{\alpha}$  is the phonon group velocity along the  $\alpha$  direction, and  $\tau_{\lambda}$  is the phonon lifetime. In bulk materials without impurities,  $\tau_{\lambda}$  is determined by the processes of two-phonon scattering from

isotopic disorder and three-phonon anharmonic scattering. In the relaxation time approximation,  $\tau_{\lambda}$  is equal to a sum of the isotope scattering rate ( $\frac{1}{\tau_{iso}}$ ) and the anharmonic scattering rate ( $\frac{1}{\tau_{anh}}$ ). For most of materials,  $\frac{1}{\tau_{iso}}$  is at least two-order smaller in magnitude than  $\frac{1}{\tau_{anh}}$ .  $\frac{1}{\tau_{anh}}$  can be calculated as the sum over  $\lambda$  of the three-phonon transition probabilities  $\Gamma_{\lambda\lambda'\lambda''}^{\pm}$ , which can be expressed as<sup>43,47-49</sup>:

$$\Gamma_{\lambda\lambda'\lambda''}^{\pm} = \frac{\hbar\pi}{8N} \left\{ \frac{2(f_{\lambda'} - f_{\lambda''})}{f_{\lambda'} + f_{\lambda''} + 1} \right\} \frac{\delta(\omega_{\lambda} \pm \omega_{\lambda'} - \omega_{\lambda''})}{\omega_{\lambda} \omega_{\lambda'} \omega_{\lambda''}} |V_{\lambda\lambda'\lambda''}^{\pm}|^2, \quad (3)$$

and

$$V_{\lambda\lambda'\lambda''}^{\pm} = \sum_{i \in u.c.} \sum_{j,k} \sum_{\alpha\beta\gamma} \frac{e_{\lambda}^{\alpha}(i) e_{p', \pm q'}^{\beta}(j) e_{p'', -q''}^{\gamma}(k)}{\sqrt{M_i M_j M_k}} \Phi_{ijk}^{\alpha\beta\gamma}, \quad (4)$$

where the upper (lower) row in curly brackets corresponds to the  $+$  ( $-$ ) sign of  $\Gamma_{\lambda\lambda'\lambda''}^{\pm}$ , which represent three-phonon absorption (two phonons merging into one phonon) and emission (one phonon splitting into two) processes. The scattering matrix elements  $V_{\lambda\lambda'\lambda''}^{\pm}$  can be evaluated with the normalized eigenvectors  $e_{p,q}$  of the three phonons involved and the anharmonic interatomic force constants (IFCs)  $\Phi_{ijk}^{\alpha\beta\gamma}$ <sup>43,49</sup>. The contribution of harmonic phonon frequencies to the anharmonic scattering rates can be represented by the three-phonon scattering phase space  $W^{\pm}$  ( $+$  and  $-$  signs corresponding to absorption and emission processes). It is defined as the sum of frequency-containing factors in the expression of three-phonon transition probabilities (Eq. 3), and is written as<sup>33</sup>:

$$W_{\lambda}^{\pm} = \frac{1}{2N} \sum_{\lambda' p''} \left\{ \frac{2(f_{\lambda'} - f_{\lambda''})}{f_{\lambda'} + f_{\lambda''} + 1} \right\} \frac{\delta(\omega_{\lambda} \pm \omega_{\lambda'} - \omega_{\lambda''})}{\omega_{\lambda} \omega_{\lambda'} \omega_{\lambda''}}. \quad (5)$$

### III. RESULTS AND DISCUSSION

Fig. 1 shows calculated  $\kappa_l$  as the function of temperature for unfilled FeSb<sub>3</sub> and CoSb<sub>3</sub><sup>50</sup>, as well as fully filled skutterudites of LaFe<sub>4</sub>Sb<sub>12</sub>, CeFe<sub>4</sub>Sb<sub>12</sub>, YbFe<sub>4</sub>Sb<sub>12</sub><sup>34</sup>, BaFe<sub>4</sub>Sb<sub>12</sub><sup>34</sup> and BaCo<sub>3</sub>Sb<sub>12</sub><sup>33</sup>. The excellent agreement between theoretical results of CoSb<sub>3</sub> and available experimental data<sup>12,51</sup> strongly indicate the validity of our calculations. Surprisingly, we find that FeSb<sub>3</sub> exhibits a quite low  $\kappa_l$  of 1.14 W/mK at 300 K, about one order of magnitude lower than 11.6 W/mK of CoSb<sub>3</sub>. In the whole temperature range the  $\kappa_l$  of FeSb<sub>3</sub> is apparently much lower than the values of the most filled skutterudites (by more than two-third). The only exception is YbFe<sub>4</sub>Sb<sub>12</sub> that owes the lowest theoretical  $\kappa_l$  among reported filled skutterudites<sup>34</sup>. The  $\kappa_l$  of FeSb<sub>3</sub> show a weak temperature dependence, resembling that of YbFe<sub>4</sub>Sb<sub>12</sub>.

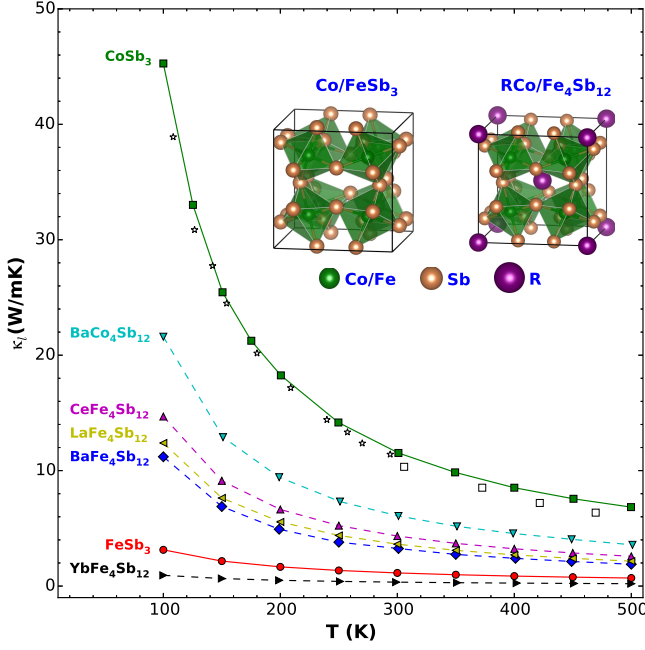


FIG. 1. (color online) Calculated temperature dependence of  $\kappa_l$  (in W/mK) of unfilled skutterudites ( $\text{FeSb}_3$ ,  $\text{CoSb}_3$ )<sup>50</sup> and several fully filled skutterudites ( $\text{LaFe}_4\text{Sb}_{12}$ ,  $\text{CeFe}_4\text{Sb}_{12}$ ,  $\text{YbFe}_4\text{Sb}_{12}$ <sup>34</sup>,  $\text{BaFe}_4\text{Sb}_{12}$ <sup>34</sup> and  $\text{BaCo}_4\text{Sb}_{12}$ <sup>33</sup>). The experimental  $\kappa_l$  for  $\text{CoSb}_3$  (open symbols) are taken from Morelli *et al.* (stars)<sup>51</sup> and Caillat *et al.* (squares)<sup>12</sup>. The inset shows crystal structures of unfilled and fully filled skutterudites.

We next elucidate the reason why  $\text{FeSb}_3$  has such an ultralow  $\kappa_l$ . The physical factors that may affect  $\kappa_l$  (see Eq. 1) include heat capacity  $C_\lambda$ , phonon velocity  $v_\lambda$  and phonon lifetime  $\tau_\lambda$  of each phonon mode  $\lambda$ . Figs. 3a and 3b show the calculated room-temperature heat capacity and the averaged group velocity over the long-wavelength acoustic phonons contributing predominately to heat-carrying, respectively. The difference in the heat capacities of  $\text{FeSb}_3$  and  $\text{CoSb}_3$  is negligibly small (less than 0.7%) and their values are  $\sim 7\%$  lower than those of  $\text{La/YbFe}_4\text{Sb}_{12}$ . This is almost exactly as expected from the Dulong-Petit law, in accord with experiments (see Fig. 2). The square of averaged phonon velocity for  $\text{FeSb}_3$  is about 17% and 10% lower than that of  $\text{CoSb}_3$  and  $\text{LaFe}_4\text{Sb}_{12}$ , respectively. This originates from the substantially reduced frequencies and velocities of the acoustic phonons in  $\text{FeSb}_3$  (see below). However, the influences of these two factors are far from enough to explain the above large discrepancies in  $\kappa_l$ . Therefore it must be the phonon lifetime that plays a central role in reducing  $\kappa_l$  of  $\text{FeSb}_3$ .

The intrinsic phonon lifetimes of crystalline materials are primarily dominated by the three-phonon anharmonic scattering processes. Fig. 4 shows the calculated anharmonic scattering rates at 300 K. As seen, the scattering rates of  $\text{FeSb}_3$  are nearly one order of magnitude larger than those of  $\text{CoSb}_3$  in the low and intermedi-

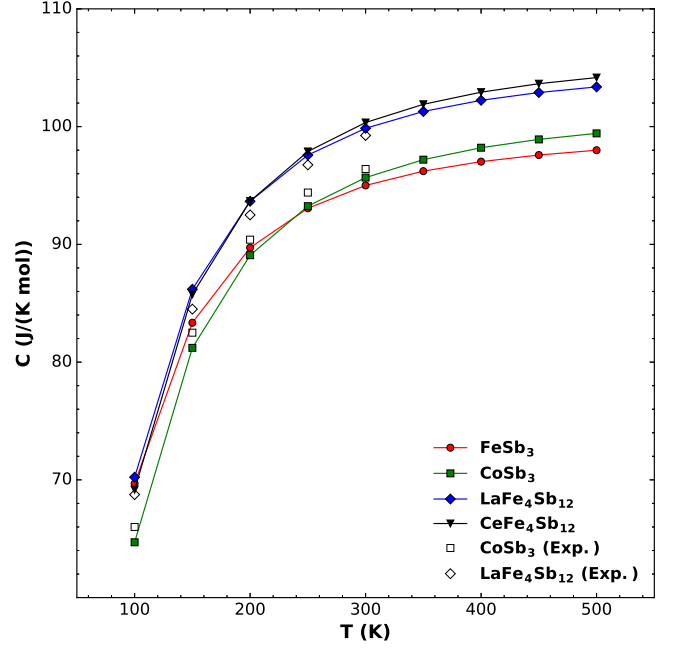


FIG. 2. (color online) Calculated heat capacity as the function of temperature for  $\text{FeSb}_3$ ,  $\text{CoSb}_3$ ,  $\text{LaFe}_4\text{Sb}_{12}$  and  $\text{CeFe}_4\text{Sb}_{12}$ . The available experimental data for  $\text{CoSb}_3$ <sup>40</sup> and  $\text{LaFe}_4\text{Sb}_{12}$ <sup>9</sup> are shown for comparison. The agreement between our calculation and the experiments is good.

ate frequency ( $\omega$ ) regions (below 5 THz). Clearly at most of  $\omega$  the rates of  $\text{FeSb}_3$  are much higher than those of  $\text{LaFe}_4\text{Sb}_{12}$ , though lower than those of  $\text{YbFe}_4\text{Sb}_{12}$ . Therefore the observed differences in the anharmonic scattering processes that limit phonon lifetimes indeed account for the discrepancies in  $\kappa_l$ . Note that the anharmonic scattering rates of  $\text{FeSb}_3$  are remarkably enhanced in a wide intermediate frequency range between  $\sim 1$  and 5 THz. The behavior is similar to those in  $\text{La/YbFe}_4\text{Sb}_{12}$  and other filled skutterudites<sup>33,34</sup>. This affects contributions of phonon modes to  $\kappa_l$ , as indicated by the cumulative plot of  $\kappa_l$  ( $\kappa_l^c$ ) that represents the fraction of heat carried by the phonons with less frequencies than  $\omega$  (inset of Fig. 4). The higher anharmonic scattering rates correspond to the smaller lifetimes, and thus the less contributions of the phonons to  $\kappa_l$ . While for  $\text{CoSb}_3$   $\kappa_l^c$  increase rapidly with  $\omega$  and the phonons below 2 THz have already contributed to  $\sim 80\%$  of  $\kappa_l$ ,  $\kappa_l^c$  of  $\text{FeSb}_3$  show a much slower increase and the phonons below 2 THz only contribute to  $\sim 50\%$  of  $\kappa_l$ . The behavior of  $\kappa_l^c$  of  $\text{FeSb}_3$  resembles those of filled skutterudites, especially  $\text{YbFe}_4\text{Sb}_{12}$ . We note that Möchel and co-workers find evidence for lattice softening in this latter compound<sup>40</sup>.

We further investigate the roles of harmonic and third-order anharmonic IFCs in enhancing three-phonon anharmonic scattering processes and reducing  $\kappa_l$  in  $\text{FeSb}_3$ . In particular we perform calculations of  $\kappa_l$  by deliberately interchanging the harmonic/anharmonic IFCs between two different compounds, as shown in Fig. 3c.

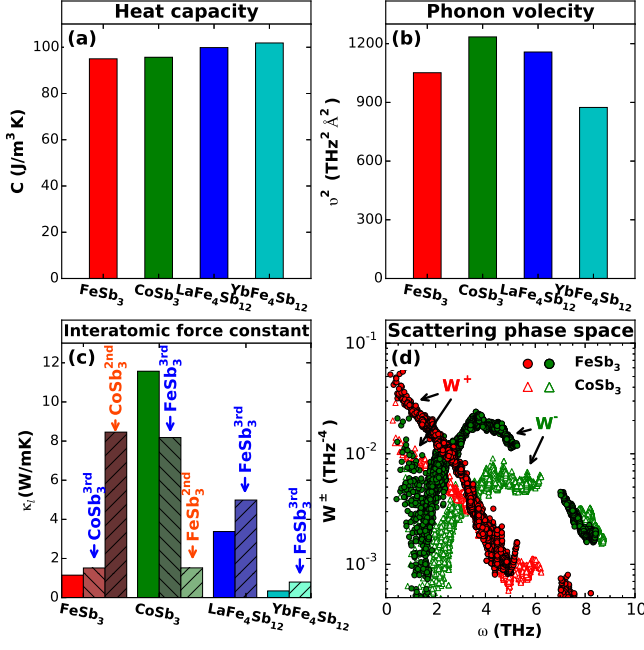


FIG. 3. (color online) Analysis of key factors that may affect  $\kappa_l$  for FeSb<sub>3</sub>, CoSb<sub>3</sub> and the filled skutterudites of La/YbFe<sub>4</sub>Sb<sub>12</sub>: (a) heat capacity, (b) phonon velocity, (c) interatomic force constant and (d) scattering phase space. In (b) the phonon velocity is calculated by averaging the group velocities of the long-wavelength (both transverse and longitudinal) acoustic phonons along different phonon momentum directions. In (c) the notation of  $M^{nth}$  represents that the  $n$ th-order IFCs of the compound M is used to replace the original IFCs when calculating the room-temperature  $\kappa_l$ .

For FeSb<sub>3</sub>, when replacing the anharmonic IFCs by the ones from CoSb<sub>3</sub> and remaining the other quantities unchanged, we find that  $\kappa_l$  increases by  $\sim 30\%$ , whereas  $\kappa_l$  of CoSb<sub>3</sub> decreases by  $\sim 30\%$  when using the anharmonic IFCs from FeSb<sub>3</sub>. The anharmonic scattering rates are generally proportional to the square of the anharmonic IFCs (Eq. 3 and 4). The result means the anharmonic IFCs of FeSb<sub>3</sub> are larger than those of CoSb<sub>3</sub>, corresponding to the higher scattering rates in FeSb<sub>3</sub>, but far from enough to account for its one-order lower  $\kappa_l$ . For the filled skutterudites of LaFe<sub>4</sub>Sb<sub>12</sub> and YbFe<sub>4</sub>Sb<sub>12</sub>, when using the anharmonic IFCs from FeSb<sub>3</sub>, the resulted  $\kappa_l$  show  $\sim 50\%$  and  $\sim 130\%$  increases, respectively. This indicates the anharmonic IFCs of FeSb<sub>3</sub> are smaller, corresponding to the lower scattering rates, which conflicts with the smaller  $\kappa_l$  of FeSb<sub>3</sub> than that of LaFe<sub>4</sub>Sb<sub>12</sub>. When we interchange the harmonic IFCs between FeSb<sub>3</sub> and CoSb<sub>3</sub>, we find  $\kappa_l$  of FeSb<sub>3</sub> increases by about 8 times, and  $\kappa_l$  of CoSb<sub>3</sub> decreases by almost the same amount. The changes accord well with the discrepancy of  $\kappa_l$  between FeSb<sub>3</sub> and CoSb<sub>3</sub>. From these results, we can conclude that the main factor responsible for the enhanced anharmonic scattering in FeSb<sub>3</sub> is the harmonic IFCs, rather than the third-order anharmonic IFCs.

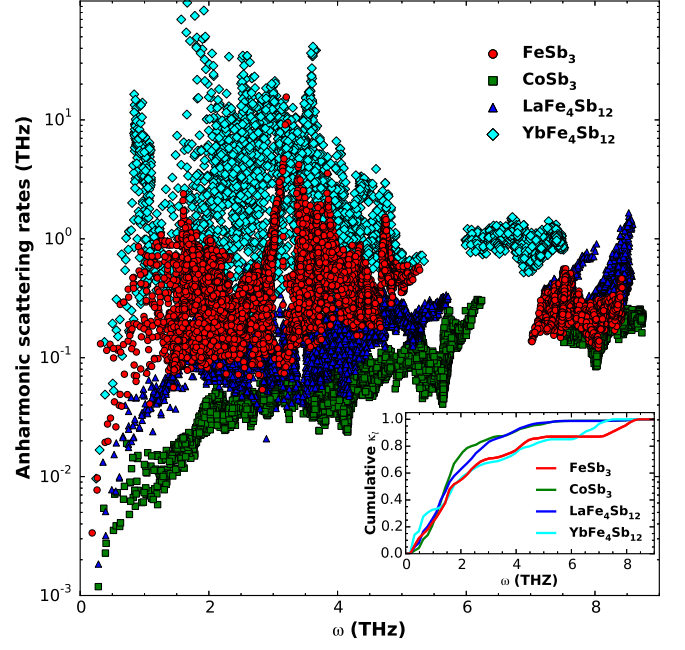


FIG. 4. (color online) Calculated anharmonic scattering rates of FeSb<sub>3</sub> (red circles), CoSb<sub>3</sub> (green squares), LaFe<sub>4</sub>Sb<sub>12</sub> (blue triangles) and YbFe<sub>4</sub>Sb<sub>12</sub> (cyan diamonds) at 300 K. The normalized cumulative  $\kappa_l$  as the function of  $\omega$  is shown in the inset.

The specific way of the harmonic IFCs affecting the anharmonic scattering processes is through phonon frequencies and eigenvectors (Eq. 3 and 4). The phonon eigenvectors contribute to the three-phonon scattering matrix elements. Usually for the same class of materials, the changes of eigenvectors with the varied harmonic IFCs are not as large as the changes of frequencies. It is thus reasonably to assume the scattering matrix elements do not change substantially here. The action of phonon frequencies on the anharmonic scattering is embodied by the three-phonon scattering phase space  $W^\pm$  (see Eq. 5), which depicts available three-phonon scattering channels among all modes. It consists of two components corresponding to absorption ( $W^+$ , two phonons merging into one) and emission ( $W^-$ , one splitting into two) processes, respectively. As show in Fig. 3d, the  $W^+$  of FeSb<sub>3</sub> are distinctly larger than those of CoSb<sub>3</sub> by several times in the low frequency ( $< 3.5$  THz) region, and the  $W^-$  of FeSb<sub>3</sub> show much larger values in the wide frequency region below 5 THz as well. The origin of the significantly enhanced  $W^\pm$  of FeSb<sub>3</sub> lies in its distinct phonon spectrum. Comparing with that of CoSb<sub>3</sub> (Fig. 5b), the phonon spectrum of FeSb<sub>3</sub> (Fig. 5a) shows a clear softening for the lowest optical branch (down to below 2 THz). This optical branch is even lower in frequency than the La-derived rattling mode in LaFe<sub>4</sub>Sb<sub>12</sub> (Fig. 5c), and is not far away from the extremely low frequency Yb-derived mode in YbFe<sub>4</sub>Sb<sub>12</sub> (cyan curve in Fig. 5c). Actually it is not only the lowest optical branch, but several adjacent



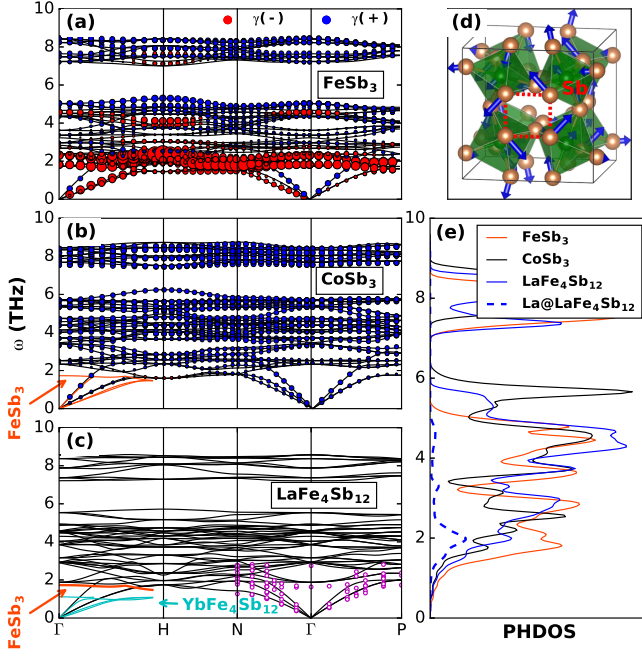


FIG. 5. (color online) (a,b,c) Calculated phonon dispersion curves of FeSb<sub>3</sub>, CoSb<sub>3</sub> and LaFe<sub>4</sub>Sb<sub>12</sub>. The size of circle represents the magnitude of Grüneisen parameter ( $\gamma$ ) for each mode, and the positive  $\gamma$  is shown in blue, negative in red. In (b) and (c) some phonon branches taken from FeSb<sub>3</sub> (in orange) and YbFe<sub>4</sub>Sb<sub>12</sub> (in cyan) are shown for comparison. For LaFe<sub>4</sub>Sb<sub>12</sub> in (c), the available experimental data from inelastic neutral scattering measurements<sup>52</sup> are shown (with magenta circles) for comparison. (d) Eigenvector of the lowest optical mode at the  $\Gamma$  point for FeSb<sub>3</sub>. The Sb<sub>4</sub> ring is indicated with red dash lines. (e) shows the (projected) phonon density of states (PHDOS).

upper optical branches that show lowering in frequency in FeSb<sub>3</sub>. This is unambiguously reflected by a sharp PHDOS peak appearing around 2 THz (Fig. 5e). It is located in the region similar to that of the La-derived rattling modes in LaFe<sub>4</sub>Sb<sub>12</sub> (blue dash line in Fig. 5e). The low-lying optical phonons overlaps more with the acoustic branches, appreciably increases the phase space  $W^\pm$  for three-phonon scattering processes (Fig. 3d). This reduces significantly phonon lifetimes, which is the main root cause for the ultralow  $\kappa_l$  of FeSb<sub>3</sub>.

Fig. 5d shows the vibration pattern of the lowest optical phonon mode of FeSb<sub>3</sub>. It involves torsion of the Sb<sub>4</sub> ring, a typical quasi-molecular motif in skutterudites. The lowering in frequency of this optical mode in FeSb<sub>3</sub> originates from the weaker Sb-Sb bonds of the Sb<sub>4</sub> ring, as demonstrated by the charge density plot in Fig. 6. Clearly the electrons in the Sb<sub>4</sub> ring of FeSb<sub>3</sub> are less localized than the case of CoSb<sub>3</sub>. This indicates the rather weaker Sb-Sb bonds in FeSb<sub>3</sub>, as expected from its electron deficient nature. This is consistent with the fact that the Young modulus of FeSb<sub>3</sub> is smaller than that of CoSb<sub>3</sub><sup>40,41</sup>. As the result, the phonon modes that

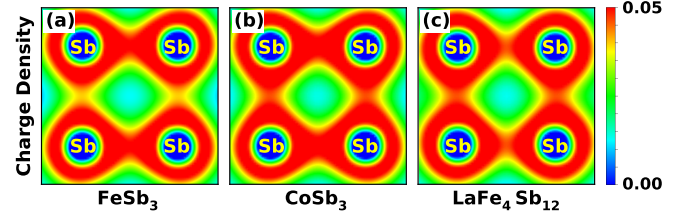


FIG. 6. (color online) Contour plot in the (100) plane of charge density on the Sb<sub>4</sub> ring (see Fig. 5d) in (a) FeSb<sub>3</sub>, (b) CoSb<sub>3</sub> and (c) LaFe<sub>4</sub>Sb<sub>12</sub>. The contour range is from 0 (blue) to 0.05 (red) electron/Å<sup>3</sup>.

are mainly dominated by Sb atoms (below 6 THz) show general softening in FeSb<sub>3</sub> (Fig. 5e). The softening also occurs to the acoustic phonons, especially the transverse modes (Fig. 5b), which leads to the moderately reduced averaged phonon velocity of FeSb<sub>3</sub> in Fig. 3b. In addition to the phonon softening, the weaker Sb-Sb bonds in FeSb<sub>3</sub> results in abnormal Grüneisen parameters ( $\gamma$ ) of phonons (Fig. 5a). For the low-lying optical branches and the transverse acoustic phonons, the values of  $\gamma$  are negative (in red) and quite large in magnitude. Such phonon modes with the large magnitude  $\gamma$  in principle facilitate high lattice anharmonicity<sup>53</sup> and thus low  $\kappa_l$ . The negative sign of  $\gamma$  for the low-lying optical branches implies that they will be further softened under contraction. This is expected to cause the more overlapping with acoustic phonons, more enhanced  $W^\pm$  and thus even lower  $\kappa_l$  at high pressures.

For the filled skutterudites, the electrons of filler transfer to the host framework following the Zintl behavior<sup>54–56</sup>. Specifically, the electropositive fillers donate charge to the more covalent transition element – Sb backbone. These electrons primarily distribute on the Sb<sub>4</sub> ring, which considerably strengthens the Sb-Sb covalent bonds, as indicated in Fig. 6c for the LaFe<sub>4</sub>Sb<sub>12</sub> case. This is consistent with the band structure of skutterudites, which shows a light Sb derived band at the top of the valence bands<sup>57</sup>. This may also explain why filled Fe-based skutterudites are easier to form than FeSb<sub>3</sub> usually stabilized in films<sup>37,39,40</sup>. If one considers only the fact that the strengthened Sb-Sb bonds after La filling lift the Sb-derived optical branches in LaFe<sub>4</sub>Sb<sub>12</sub>, an increase of  $\kappa_l$  is expected. In fact, the La filler derived rattling modes take the role to remarkably enhance  $W^\pm$ . As the result  $\kappa_l$  of LaFe<sub>4</sub>Sb<sub>12</sub> is still much lower than that of CoSb<sub>3</sub>, and only about three times larger than that of FeSb<sub>3</sub>. For the case of YbFe<sub>4</sub>Sb<sub>12</sub>, the Yb derived even lower frequency and rather flat optical phonon branches increase  $W^\pm$  more significantly, resulting in the more reduced  $\kappa_l$ <sup>34</sup>. Note that flat optical branches generally have large phase space for Umklapp scattering, but by themselves do not carry substantial heat regardless.

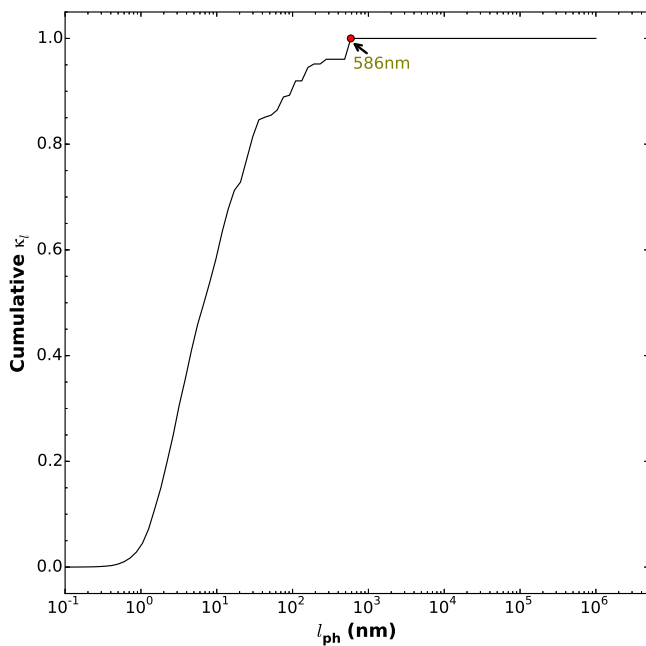


FIG. 7. (color online) The normalized cumulative  $\kappa_l$  of FeSb<sub>3</sub> as a function of the phonon mean free path ( $l_{ph}$ ) at 300 K. The maximum  $l_{ph}$  among all the modes, which corresponds to the onset point of the cumulative  $\kappa_l$  becoming constant (equal to 1.0), is indicated.

#### IV. CONCLUSIONS

To summarize, we report a discovery of ultralow  $\kappa_l$  in pure skutterudite FeSb<sub>3</sub> with no filler by using first principles Boltzmann-Peierls transport simulations. The calculated  $\kappa_l$  is only 1.14 W/mK at room temperature, one order of magnitude lower than that of CoSb<sub>3</sub>. It is even lower than the  $\kappa_l$  of most of fully filled skutterudites. This is in contrast to the widely used approach where filling is used for reduction of  $\kappa_l$  in skutterudites.

The origin of the ultralow  $\kappa_l$  is attributed to the optical phonons with remarkable lowering in frequency associated with the weaker Sb-Sb bonds in FeSb<sub>3</sub> owing to its electron deficient nature. These low-frequency optical phonons take the role of the rattling modes in filled skutterudites. Particularly they overlap more with the heat-carrying acoustic phonons and increase the phase space of three-phonon anharmonic scattering processes, resulting in significantly reduced phonon lifetimes and thus ultralow  $\kappa_l$ . Our results offer new insight into the still debated mechanism responsible for the  $\kappa_l$  reduction upon filling in skutterudites and also a new routine for lowering  $\kappa_l$  of skutterudite-type thermoelectric materials. Finally we evaluate the maximum mean free path of phonons ( $l_{ph}$ ) for bulk FeSb<sub>3</sub>, as shown in Fig. 7. The purpose of such calculation is to provide a reference to future experimental measurements for how thick thin-film samples are required to take on the intrinsic  $\kappa_l$  of bulk FeSb<sub>3</sub> we calculated here. According to our result, the maximum  $l_{ph}$  is less than 600 nm. The sample size above this value is needed to safely avoid surface and grain boundary scatterings. Therefore the experimentally synthesized FeSb<sub>3</sub> films with the thicknesses of 1.0-1.5  $\mu\text{m}$ <sup>40</sup> may be directly applied to measure the intrinsic  $\kappa_l$  and verify our theoretical prediction.

#### ACKNOWLEDGMENTS

The authors acknowledge funding support from the Recruitment Program of Global Youth Experts in China and special funds for talent development in Jilin Province. Part of calculations was performed in the high performance computing center of Jilin University and on TianHe-1 (A) of National Supercomputer Center in Tianjin. Work of D.J.S. is supported by S3TEC an Energy Frontier Research Center funded by the Department of Energy, Office of Science, Basic Energy Sciences under award #DE-SC0001299 / DE-FG02-09ER46577.

\* wu.li.phys2011@gmail.com

† lijun\_zhang@jlu.edu.cn

<sup>1</sup> D. T. Morelli and G. P. Meisner, J. Appl. Phys. **77**, 3777 (1995).

<sup>2</sup> B. C. Sales, D. Mandrus, and R. K. Williams, Science **272**, 1325 (1996).

<sup>3</sup> G. S. Nolas, D. T. Morelli, and T. M. Tritt, Annu. Rev. Mater. Sci. **29**, 89 (1999).

<sup>4</sup> X. Shi, J. Yang, J. R. Salvador, M. Chi, J. Y. Cho, H. Wang, S. Bai, J. Yang, W. Zhang, and L. Chen, J. Am. Chem. Soc. **133**, 7837 (2011).

<sup>5</sup> D. J. Singh and I. I. Mazin, Phys. Rev. B **56**, R1650 (1997).

<sup>6</sup> W. Zhang, X. Shi, Z. G. Mei, Y. Xu, L. D. Chen, J. Yang, and G. P. Meisner, Appl. Phys. Lett. **89**, 112105 (2006).

<sup>7</sup> D. T. Morelli, G. P. Meisner, B. Chen, S. Hu, and C. Uher, Phys. Rev. B **56**, 7376 (1997).

<sup>8</sup> G. Rogl, A. Grytsiv, E. Bauer, P. Rogl, and M. Zehetbauer, Intermetallics **18**, 57 (2010).

<sup>9</sup> W. Schnelle, A. Leithe-Jasper, H. Rosner, R. Cardoso-Gil, R. Gumeniuk, D. Trots, J. A. Mydosh, and Y. Grin, Phys. Rev. B **77**, 094421 (2008).

<sup>10</sup> H. Li, X. Tang, Q. Zhang, and C. Uher, Appl. Phys. Lett. **94**, 102114 (2009).

<sup>11</sup> J. S. Dyck, W. Chen, C. Uher, L. Chen, X. Tang, and T. Hirai, J. Appl. Phys. **91**, 3698 (2002).

<sup>12</sup> T. Caillat, A. Borshchevsky, and J. Fleurial, J. Appl. Phys. **80**, 4442 (1996).

<sup>13</sup> J. Yang and T. Caillat, MRS Bull. **31**, 224 (2006).

<sup>14</sup> J. Yang, P. Qiu, R. Liu, L. Xi, S. Zheng, W. Zhang, L. Chen, D. J. Singh, and J. Yang, Phys. Rev. B **84**, 235205 (2011).

- <sup>15</sup> G. S. Nolas, M. Kaeser, R. T. Littleton, and T. M. Tritt, *Appl. Phys. Lett.* **77**, 1855 (2000).
- <sup>16</sup> L. D. Chen, T. Kawahara, X. F. Tang, T. Goto, T. Hirai, J. S. Dyck, W. Chen, and C. Uher, *J. Appl. Phys.* **90**, 1864 (2001).
- <sup>17</sup> G. A. Lamberton, S. Bhattacharya, R. T. Littleton, M. A. Kaeser, R. H. Tedstrom, T. M. Tritt, J. Yang, and G. S. Nolas, *Appl. Phys. Lett.* **80**, 598 (2002).
- <sup>18</sup> L. Zhang, A. Grytsiv, P. Rogl, E. Bauer, and M. Zehetbauer, *J. Phys. D: Appl. Phys.* **42**, 225405 (2009).
- <sup>19</sup> G. Rogl, A. Grytsiv, P. Rogl, N. Peranio, E. Bauer, M. Zehetbauer, and O. Eibl, *Acta Mater.* **63**, 30 (2014).
- <sup>20</sup> J. Yang, L. Xi, W. Qiu, L. Wu, X. Shi, L. Chen, J. Yang, W. Zhang, C. Uher, and D. J. Singh, *npj Comput. Mater.* **2**, 15015 (2016).
- <sup>21</sup> G. A. Slack, in *CRC Handbook of Thermoelectrics*, edited by D. M. Rowe (CRC Press, Boca Raton, FL, 1995) pp. 402–406.
- <sup>22</sup> X. Y. Zhao, X. Shi, L. D. Chen, W. Q. Zhang, W. B. Zhang, and Y. Z. Pei, *J. Appl. Phys.* **99**, 053711 (2006).
- <sup>23</sup> Y. Z. Pei, L. D. Chen, W. Zhang, X. Shi, S. Q. Bai, X. Y. Zhao, Z. G. Mei, and X. Y. Li, *Appl. Phys. Lett.* **89**, 221107 (2006).
- <sup>24</sup> P. F. Qiu, J. Yang, R. H. Liu, X. Shi, X. Y. Huang, G. J. Snyder, W. Zhang, and L. D. Chen, *J. Appl. Phys.* **109**, 063713 (2011).
- <sup>25</sup> G. A. Slack and V. G. Tsoukala, *J. Appl. Phys.* **76**, 1665 (1994).
- <sup>26</sup> V. Keppens, D. Mandrus, B. Sales, B. Chakoumakos, P. Dai, R. Coldea, M. Maple, D. Gajewski, E. Freeman, and S. Bennington, *Nature* **395**, 876 (1998).
- <sup>27</sup> R. P. Hermann, R. Jin, W. Schweika, F. Grandjean, D. Mandrus, B. C. Sales, and G. J. Long, *Phys. Rev. Lett.* **90**, 135505 (2003).
- <sup>28</sup> H.-C. Wille, R. P. Hermann, I. Sergueev, O. Leupold, P. van der Linden, B. C. Sales, F. Grandjean, G. J. Long, R. Rüffer, and Y. V. Shvyd'ko, *Phys. Rev. B* **76**, 140301 (2007).
- <sup>29</sup> M. M. Koza, M. R. Johnson, R. Viennois, H. Mutka, L. Girard, and D. Ravot, *Nat. Mater.* **7**, 805 (2008).
- <sup>30</sup> J. L. Feldman, D. J. Singh, I. I. Mazin, D. Mandrus, and B. C. Sales, *Phys. Rev. B* **61**, R9209 (2000).
- <sup>31</sup> A. Yamakage and Y. Kuramoto, *J. Phys. Soc. Jpn.* **78**, 064602 (2009).
- <sup>32</sup> N. Bernstein, J. L. Feldman, and D. J. Singh, *Phys. Rev. B* **81**, 134301 (2010).
- <sup>33</sup> W. Li and N. Mingo, *Phys. Rev. B* **89**, 184304 (2014).
- <sup>34</sup> W. Li and N. Mingo, *Phys. Rev. B* **91**, 144304 (2015).
- <sup>35</sup> B. C. Sales, D. Mandrus, B. C. Chakoumakos, V. Keppens, and J. R. Thompson, *Phys. Rev. B* **56**, 15081 (1997).
- <sup>36</sup> C. H. Lee, I. Hase, H. Sugawara, H. Yoshizawa, and H. Sato, *J. Phys. Soc. Jpn.* **75**, 123602 (2006).
- <sup>37</sup> M. V. Daniel, L. Hammerschmidt, C. Schmidt, F. Timmermann, J. Franke, N. Jöhrmann, M. Hietschold, D. C. Johnson, B. Paulus, and M. Albrecht, *Phys. Rev. B* **91**, 085410 (2015).
- <sup>38</sup> G. Xing, X. Fan, W. Zheng, Y. Ma, H. Shi, and D. J. Singh, *Sci. Rep.* **5** (2015).
- <sup>39</sup> M. D. Hornbostel, E. J. Hyer, J. Thiel, and D. C. Johnson, *J. Am. Chem. Soc.* **119**, 2665 (1997).
- <sup>40</sup> A. Möchel, I. Sergueev, N. Nguyen, G. J. Long, F. Grandjean, D. C. Johnson, and R. P. Hermann, *Phys. Rev. B* **84**, 064302 (2011).
- <sup>41</sup> M. Räsander, L. Bergqvist, and A. Delin, *Phys. Rev. B* **91**, 014303 (2015).
- <sup>42</sup> S. Lemal, N. Nguyen, J. de Boer, P. Ghosez, J. Varignon, B. Klobes, R. P. Hermann, and M. J. Verstraete, *Phys. Rev. B* **92**, 205204 (2015).
- <sup>43</sup> W. Li, J. Carrete, N. A. Katcho, and N. Mingo, *Comput. Phys.* **185**, 1747 (2014).
- <sup>44</sup> P. E. Blöchl, *Phys. Rev. B* **50**, 17953 (1994).
- <sup>45</sup> G. Kresse and J. Furthmüller, *Phys. Rev. B* **54**, 11169 (1996).
- <sup>46</sup> A. Togo, F. Oba, and I. Tanaka, *Phys. rev. B* **78**, 134106 (2008).
- <sup>47</sup> D. A. Broido, M. Malorny, G. Birner, N. Mingo, and D. A. Stewart, *Appl. Phys. Lett.* **91**, 231922 (2007).
- <sup>48</sup> A. Ward, D. A. Broido, D. A. Stewart, and G. Deinzer, *Phys. Rev. B* **80**, 125203 (2009).
- <sup>49</sup> W. Li, L. Lindsay, D. A. Broido, D. A. Stewart, and N. Mingo, *Phys. Rev. B* **86**, 174307 (2012).
- <sup>50</sup> W. Li and N. Mingo, *Phys. Rev. B* **90**, 094302 (2014).
- <sup>51</sup> D. T. Morelli, T. Caillat, J.-P. Fleurial, A. Borshchevsky, J. Vandersande, B. Chen, and C. Uher, *Phys. Rev. B* **51**, 9622 (1995).
- <sup>52</sup> M. M. Koza, M. Boehm, E. Sischka, W. Schnelle, H. Mutka, and A. Leithe-Jasper, *Phys. Rev. B* **91**, 014305 (2015).
- <sup>53</sup> J. S. Dugdale and D. K. C. MacDonald, *Phys. Rev.* **98**, 1751 (1955).
- <sup>54</sup> D. Braun and W. Jeitschko, *J. Less Common Metals* **72**, 147 (1980).
- <sup>55</sup> G. A. Papoian and R. Hoffmann, *Angew. Chem. Int. Ed.* **39**, 2408 (2000).
- <sup>56</sup> H. Luo, J. W. Krizan, L. Muechler, N. Haldolaarachchige, T. Klimczuk, W. Xie, M. K. Fuccillo, C. Felser, and R. J. Cava, *Nat. Commun.* **6** (2015).
- <sup>57</sup> D. J. Singh and W. E. Pickett, *Phys. Rev. B* **50**, 11235 (1994).